Science and Technology for the Built Environment

ISSN: (Print) (Online) Journal homepage: https://www.tandfonline.com/loi/uhvc21

Role of receiver on the performance of a transcritical CO_2 based air-conditioning unit with single-stage and two-stage expansion

Mihir Mouchum Hazarika, Maddali Ramgopal, Souvik Bhattacharyya & Rodrigo Llopis Doménech

To cite this article: Mihir Mouchum Hazarika, Maddali Ramgopal, Souvik Bhattacharyya & Rodrigo Llopis Doménech (2021): Role of receiver on the performance of a transcritical CO_2 based air-conditioning unit with single-stage and two-stage expansion, Science and Technology for the Built Environment, DOI: 10.1080/23744731.2021.1902189

To link to this article: https://doi.org/10.1080/23744731.2021.1902189

Published online: 22 Mar 2021.

Science and Technology for the Built Environment, (2021) **0**, 1–28

ISSN: print / online
DOI: 10.1080/23744731.2021.1902189

Role of receiver on the performance of a transcritical CO_2 based air-conditioning unit with single-stage and two-stage expansion

MIHIR MOUCHUM HAZARIKA[1]*, MADDALI RAMGOPAL[2], SOUVIK BHATTACHARYYA[3], and RODRIGO LLOPIS DOMÉNECH[4]

[1]*Department of Energy and Process Engineering, Norwegian University of Science and Technology, Trondheim, Norway*
[2]*Department of Mechanical Engineering, IIT Kharagpur, Kharagpur, India*
[3]*Department of Mechanical Engineering, BITS Pilani, Pilani, India*
[4]*Department of Mechanical Engineering and Construction, Jaume I University, Castelló, Spain*

Theoretical and experimental studies are carried out on a transcritical CO_2 based air-conditioning unit. Two configurations– a system with single-stage expansion (SSE) and a system with two-stage expansion (TSE) have been considered. Detailed numerical models have been developed for both configurations. Results obtained from numerical simulations are compared with experimental results. The performance of the system with single-stage expansion is compared with two-stage expansion under different conditions of refrigerant charge, receiver volume, and ambient temperature. Both numerical and experimental results show that the SSE configuration is highly sensitive to refrigerant charge as compared to the TSE configuration. The TSE configuration offers better system controllability provided the receiver is sized properly. Besides, it is found that for the same performance, the required charge can be reduced by about 15% for the TSE configuration as compared to the SSE configuration.

Introduction

With the rising concerns about global warming, the use of harmful synthetic refrigerants with high global warming potential (GWP) is no longer encouraged. Environment-friendly, natural refrigerants are seen as permanent replacements for the high GWP, synthetic refrigerants. Hydrocarbons have been widely used in recent years for small capacity refrigeration and air-conditioning applications. However, hydrocarbons are flammable. Though ammonia is an excellent refrigerant and is widely used, it is toxic and suffers from material compatibility issues. Carbon dioxide (CO_2), being non-flammable as well as nontoxic, is considered as a promising natural refrigerant due to its excellent thermophysical properties and material compatibility. However, CO_2 has a comparatively low critical temperature ($\approx 31\,^{\circ}C$). Lorentzen and Pettersen (1993) have shown the possibility of using CO_2 in a transcritical refrigeration cycle by developing a system for air-conditioning application, thereby overcoming the operational difficulties associated with the low critical temperature of CO_2.

The performance of a single-stage transcritical CO_2 based system drops at high ambient temperature. To enhance the performance of transcritical CO_2 based system, extensive studies have been carried out in recent years. Different modifications have been proposed for the CO_2 system. The use of an ejector as an expansion work recovering device, use of parallel compression, and use of mechanical subcooling are considered as effective solutions to enhance the performance of the transcritical CO_2 system. Groll and Kim (2007) carried out an extensive review to analyze the potential benefits of using different modifications to enhance the performance of a transcritical CO_2 system. These modifications are the use of two-stage compression, use of work recovering expander, use of vortex tube as an expansion device, use of ejector as an expansion device, and use of thermoelectric subcooling device to enhance the performance of the CO_2 system. They observed that the two-stage cycle with intercooling gave the highest energy efficiency. Lawrence and Elbel (2015) carried out studies to compare the performance of a CO_2 ejector with an R134a ejector. They observed that

Received August 16, 2020; accepted March 4, 2021
Mihir Mouchum Hazarika, PhD, is a Postdoctoral Fellow. **Maddali Ramgopal, PhD**, is a Professor. **Souvik Bhattacharyya, PhD**, is a Senior Professor and Vice-Chancellor. **Rodrigo Llopis Doménech, PhD**, is a Professor.
*Corresponding author e-mail: mihir.m.hazarika@ntnu.no

the CO_2 ejector performed better as compared to the R134a ejector. Later, Elbel and Lawrence (2016) presented an extensive review on the use of an ejector as an expansion work recovering device in the transcritical CO_2 system. They reported that improvement in COP is in the range of 10 to 30% for transcritical CO_2 systems with ejectors. In a recent study, Zhu and Elbel (2020) introduced a new method in which a vortex was generated in the motive flow of CO_2 ejector to regulate the high-side pressure. They reported that the use of this vortex control method in the CO_2 ejector improved the system COP and capacity by 8.1% and 11.0%, respectively under off-design conditions. Cao, Ye, and Wang (2020) carried out an experimental study to analyze the effects of using an internal heat exchanger in a transcritical CO_2 heat pump. Karampour and Sawalha (2018) showed the potential benefits of using parallel compression and mechanical subcooling in a transcritical CO_2 booster system. Bush et al. (2017) conducted experimental studies to investigate the performance of a transcritical CO_2 booster system with mechanical subcooling. They reported that the use of mechanical subcooling significantly improved the performance and reduced the amount of flash gas in the flash tank. Catalán-Gil et al. (2019) carried out studies to compare the energy improvements gained by using integrated and dedicated mechanical subcooling in a transcritical CO_2 booster system. In a recent experimental study, Nebot-Andrés et al. (2020) estimated the optimum operating conditions of a transcritical CO_2 system with integrated mechanical subcooling. All these studies presented here showed that CO_2 systems could provide long term energy-efficient solutions, provided the issues related to performance are suitably addressed.

Unlike conventional refrigeration cycles, the transcritical refrigeration cycle needs a suitable control scheme to optimize the high side pressure owing to the peculiar shape of the isotherm in the supercritical region. Several control schemes have been proposed to optimize the high side pressure for a CO_2 based system. Few studies reported methods to optimize the high side pressure by regulating the speed of the gas cooler fan (Baek et al. 2013). For such a system, the high side pressure can also be optimized by using an electronic expansion valve (Cho, Ryu, and Kim 2007; Hou et al. 2014). Although, single expansion valve can effectively maintain the optimum high side pressure of a transcritical CO_2 based system; it is not possible to maintain the desired refrigerant flowrate at the evaporator simultaneously to maintain the degree of superheat. Casson et al. (2003) suggested a novel method of using two expansion valves with a receiver in between for simultaneous control of gas cooler pressure as well as the degree of superheat. This particular control strategy has been found more reliable in optimizing the performance of CO_2 based systems (Boccardi et al. 2013; Cabello et al. 2008; Llopis et al. 2016). Most of the commercial CO_2 systems designed for supermarkets are now equipped with this control strategy using two-stage expansion (Gullo, Hafner, and Banasiak 2018). However, the detailed theoretical and experimental studies on systems using two EEVs and their performance comparison with single EEV are scarce in the literature.

A detailed literature survey reveals that even though several mathematical models have been proposed to simulate the performance of CO_2 based transcritical systems (Lin et al. 2013), the effect of refrigerant charge on system performance is not considered by many. The impact of the refrigerant charge on system performance is very important, especially in mobile air conditioning applications where the refrigerant leakage rates are typically very high. Refrigerant leakages are also relatively high in small split air conditioning systems. Since depletion of refrigerant is expected to affect the performance of critically charged systems such as the ones mentioned, it is important to carry out studies to evaluate the same. Cho et al. (2005) carried out an experimental study to compare the performance of a transcritical CO_2 system with R22, R410A, and R407C systems. They reported that the CO_2 system showed the highest sensitivity in performance to change in refrigerant charge. Moreover, the performance was found to be deteriorating significantly at undercharged conditions. Hazarika, Ramgopal, and Bhattacharyya (2018) developed a numerical model for a transcritical CO_2 based air-conditioning system and carried out experiments to validate the model. The numerical results showed that the COP of the system drops marginally for ±18% change from the optimum refrigerant charge. However, any change in charge beyond this range affects the performance significantly. Wang et al. (2019) performed an experimental study to optimize the refrigerant charge for a transcritical CO_2 system for heating application. They also reported the effect of system transient on the migration of refrigerant charge. These studies show the importance of refrigerant charge for operating the system at optimum conditions. It is seen that very limited studies are available in the literature on the performance of single-stage expansion vis-a-vis two-stage expansion in transcritical CO_2 systems.

The objective of the present study is to investigate the performance of a transcritical CO_2 based system. The intended applications of the system studied are in the field of small capacity (around 3.5 to 7 kW) systems for residential and mobile air conditioning. Two configurations are selected for the proposed CO_2 system: one configuration employs a single expansion valve while the other employs double expansion valves. The primary goal of this study is to compare the performance of the proposed configurations. For the configuration with two-stage expansion, a receiver must be located between the two expansion valves. The impact of the size of the receiver on system performance is also analyzed in the present study. To fulfill these objectives, experimental tests and numerical simulations are carried out for both configurations. The influences of refrigerant charge, receiver volume, and ambient temperature on system performance are presented and analyzed in the results.

Control strategies with expansion device for transcritical CO_2 cycle

One of the commonly used techniques to control the high-side pressure for transcritical CO_2 cycle is to use an

electronic expansion valve driven by a feedback controller. The feedback controller adjusts the cross-sectional area of the expansion valve opening to maintain the desired high-side pressure. However, with this control strategy, it is not possible simultaneously to feed the evaporator with the desired refrigerant flowrate and control the heat rejection pressure. For such configuration, an accumulator as a suction line heat exchanger should be located before the compressor and this accumulator could be flooded partially with liquid refrigerant. Lorentzen and Pettersen (1993) suggested that the accumulator helps in supplying the necessary refrigerant flowrate to the evaporator under varying operating conditions.

Traditionally, a single expansion valve (mechanical or electronic) is used in a refrigeration system to maintain the desired degree of superheat at the evaporator exit. When this approach is adopted for the transcritical CO_2 cycle, to maintain the desired high-side pressure, a given system has to be charged with an optimum amount of refrigerant for a specific operating condition (Aprea, Greco, and Maiorino 2015; Cho et al. 2005; Hazarika, Ramgopal, and Bhattacharyya 2018). However, when the operating conditions change due to change in heat source or sink temperature and/or refrigeration load, the resulting high-side pressure may deviate from the desired optimum high-side pressure, resulting in sub-optimal performance.

Hence in a transcritical cycle, to control the high-side pressure and degree of superheat simultaneously for maximum COP, the use of two-stage expansion with a receiver in between is suggested by Casson et al. (2003). It is shown that the first expansion valve plays the role of a differential expansion valve that maintains the receiver pressure as well as the differential pressure drop. The receiver is always maintained at saturation pressure such that saturated liquid exists at the outlet of the differential valve. The second expansion valve maintains the degree of superheat by feeding the evaporator with the required refrigerant flowrate. Thus it is possible to maintain the high-side pressure as well as the degree of superheat simultaneously. During operation, the receiver is kept partially flooded with liquid refrigerant. Casson et al. (2003) suggested that, with this control strategy, it is possible to achieve optimum performance for the transcritical cycle under varying operating conditions. However, it is essential to predict the size of the receiver as well as the amount of refrigerant charge appropriately to maintain sufficient liquid in the receiver under varying operating conditions. These issues are addressed in the present work.

Experimental test facility

An experimental test facility is built to study the performance of the system with single and two-stage expansion. The test-rig comprises of fin-and-tube type evaporator and gas cooler, electronic expansion valves, a receiver, an accumulator, and a semi-hermetic compressor. A photograph and schematic drawing of the test-rig are shown in Figure 1. Tests are conducted to investigate the sensitivity of the performance of the system to refrigerant charge with two-stage and single-stage expansion. Then by comparing the results, it is observed that the numerical results agree reasonably well with the experimental results. The maximum uncertainty in cooling capacity and gas cooler heat rejection rates are estimated to be 8.7% and 9.6%, respectively. The detailed description of the test facility is presented in earlier communication by the authors (Hazarika, Ramgopal, and Bhattacharyya 2018).

Simulation model

A mathematical model is developed to simulate the performance of the experimental test-rig shown in Figure 1. The steady-state model presented in this manuscript has similarities with the model presented in the earlier communication (Hazarika, Ramgopal, and Bhattacharyya 2018). This model is developed by integrating the models for individual components. The individual component models are adopted from the earlier manuscript (Hazarika, Ramgopal, and Bhattacharyya 2018). In the earlier case, the steady-state model is developed considering a single expansion valve that is used to maintain the desired degree of superheat. In the present study, the steady-state model for the CO_2 system is upgraded considering double expansion valves- the first one maintains the desired high-side pressure while the second one maintains the desired degree of superheat. Finally, numerical simulations are carried out for both configurations: single-stage expansion system and two-stage expansion system.

In case of the configuration with two-stage expansion, the high-pressure fluid that leaves the gas cooler is expanded in the first-stage (EEV1). After the first stage of expansion, the fluid enters the receiver. The fluid exiting the receiver is then expanded in the second-stage (EEV2). On the other hand, in the case of the configuration with a single-stage of expansion, the first stage of expansion is bypassed as shown in Figure 1b.

Compressor

The compressor is modeled assuming an irreversible, but adiabatic compression process. Empirical correlations for isentropic and volumetric efficiencies of the compressor suggested by Wang et al. (2013) are used to predict the power input to the compressor and mass flow rate of the refrigerant. For the sake of simplification, the refrigerant present in the compressor is neglected in the present model. However, the amount of refrigerant present in the compressor can be estimated by considering the single-phase vapor present in the shell side of the compressor and the liquid refrigerant dissolved in the lubricating oil (He et al. 2020). It is observed that this amount is less than 2% of the total refrigerant charge. This is due to the presence of two pressure vessels, the receiver and accumulator, which contain a major portion of the refrigerant charge. Hence, this amount

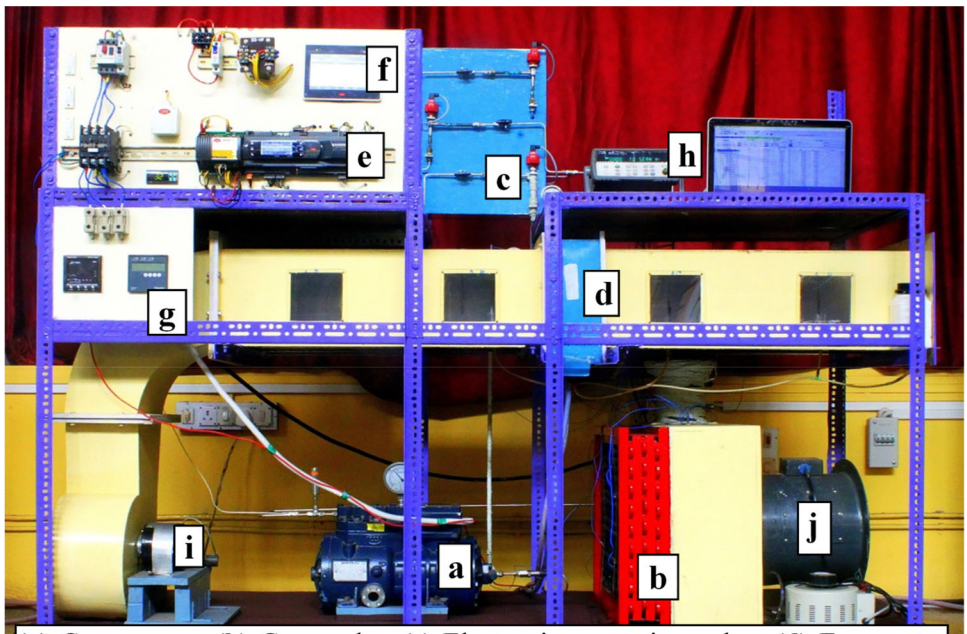

(a) Compressor, **(b)** Gas cooler, **(c)** Electronic expansion valve, **(d)** Evaporator with duct, **(e)** Controller, **(f)** Display unit, **(g)** Energy meter, **(h)** Data acquisition system, **(i)** Evaporator fan, **(j)** Gas cooler fan

(a)

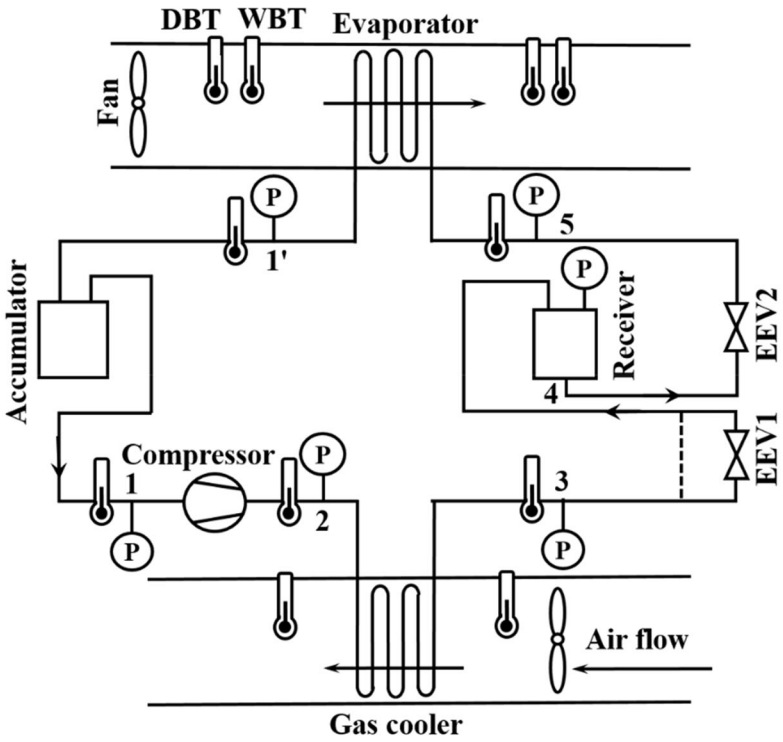

(b)

Fig. 1. (a) Photograph and (b) schematic of the CO_2 based air conditioning unit.

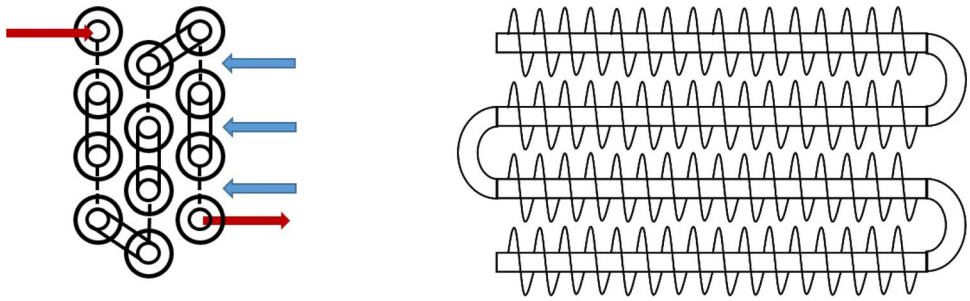

(a) (b)

Fig. 2. Schematic of (a) arrangement of tubes, and (b) single tube row of a spiral-fin-and-tube heat exchanger.

of charge present in the compressor is neglected in this study.

Gas cooler

The gas cooler is a fin-and-tube heat exchanger with spiral fins as shown in Figure 2. Air and refrigerant approach the gas cooler from the opposite direction as the counter-cross flow arrangement is chosen. This gas cooler is modeled using energy balance equations for the air and refrigerant side with suitable empirical correlations for heat transfer and pressure drop available in the literature. Considering the steep property variation on the CO_2 side, the entire gas cooler is discretized into finite elements (Yin, Bullard, and Hrnjak 2001) and the governing equations are applied across each element. An iterative procedure is adopted to find the outlet conditions of the gas cooler from known inlet conditions on air and refrigerant sides. The equations are solved numerically using an element size that leads to a grid-independent solution.

For each element, heat transfer rate is expressed as:

$$\begin{aligned}\Delta Q &= \varepsilon \times C_{min} \times \left(T_{ref}(i,j,k) - T_a(i,j,k)\right) \\ &= \dot{m}_a \times C_{p_a} \times \left(T_{a,ex}(i,j,k) - T_{a,in}(i,j,k)\right) \\ &= \dot{m}_{ref} \times \left(h_{ref}(i+1,j,k) - h_{ref}(i,j,k)\right)\end{aligned} \tag{1}$$

for

$$C_{max} = C_{CO_2};\ \ \varepsilon = 1 - \exp\left(-\gamma \frac{C_{max}}{C_{min}}\right) \tag{2}$$

where,

$$\gamma = 1 - \exp\left(-\frac{UA}{C_{max}}\right) \tag{3}$$

for

$$C_{min} = C_{CO_2};\ \ \varepsilon = \frac{C_{max}}{C_{min}}\left(1 - \exp\left(-\gamma \frac{C_{min}}{C_{max}}\right)\right) \tag{4}$$

where,

$$\gamma = 1 - \exp\left(-\frac{UA}{C_{min}}\right) \tag{5}$$

$$\frac{1}{UA} = \frac{1}{\alpha_a \times \eta_{overall} \times a_{node}} + \frac{1}{\alpha_{ref} \times a_i} \tag{6}$$

The heat transfer coefficient of CO_2 during the heat exchange process in the gas cooler is estimated using the correlation proposed by Pitla, Groll, and Ramadhyani (2002):

$$\alpha_i = \frac{Nu}{d_i} \times k_{ref} \tag{7}$$

$$Nu = \left(\frac{Nu_{wall} + Nu_{bulk}}{2}\right)\frac{k_{wall}}{k_{bulk}} \tag{8}$$

where "Nu_{wall}" and "Nu_{bulk}" are Nusselt numbers calculated at the wall and bulk temperatures. These two parameters "Nu_{wall}" and "Nu_{bulk}" are calculated using Gnielinski correlation within the range $2300 < \mathrm{Re} < 10^6$ and $0.6 < \mathrm{Pr} < 10^5$:

$$Nu = \frac{(f/8)(\mathrm{Re} - 1000)\mathrm{Pr}}{12.7\sqrt{f/8}(\mathrm{Pr}^{2/3} - 1) + 1.07} \tag{9}$$

For $\mathrm{Re} > 10^6$, Petukhov–Popov–Kirilov correlation is used to calculate "Nu_{wall}" and "Nu_{bulk}":

$$Nu = \frac{(f/8)\mathrm{RePr}}{12.7\sqrt{f/8}(\mathrm{Pr}^{2/3} - 1) + 1.07} \tag{10}$$

where friction factor 'f' is given by:

$$f = (0.79\ln(\mathrm{Re}) - 1.64)^{-2} \tag{11}$$

To estimate the heat transfer coefficient and pressure drop on air-side, the Colburn factor "j" and friction factor "f" are estimated. Pongsoi et al. (2013) suggested correlations to estimate these parameters for a fin-and-tube heat exchanger with spiral fins:

$$j = 0.2150 \times \mathrm{Re}_{d_o}^{-0.4059} \tag{12}$$

$$f = 0.4852 \times \mathrm{Re}_{d_o}^{-0.2156} \times \left(\frac{f_p}{d_o}\right)^{0.4771} \tag{13}$$

Evaporator

Similar to the gas cooler, the evaporator is also modeled using a finite element approach. As the evaporator operates at subcritical pressure with a finite degree of superheat at

the exit, both single-phase and two-phase zones exist inside the evaporator tubes. Also depending upon the outer surface temperature, moisture from the air can condense (wet coil) or does not condense (dry coil). The heat and mass transfer phenomena occurring on the evaporator coil is modeled using Threlkeld (1970) method. Suitable equations are used to estimate the heat transfer coefficients and pressure drop in single as well as two-phase regions. Using the model, the latent and sensible heat transfer rates on the air side are estimated, which are required to calculate the dry-bulb temperature and moisture content of air at the evaporator exit.

For each wet element, heat transfer rate is estimated from (Threlkeld 1970):

$$\begin{aligned}\Delta Q &= \dot{m}_a \times (h_{a,ex} - h_{a,in}) \\ &= \dot{m}_{ref} \times \left(h_{ref}(i,j,k) - h_{ref}(i+1,j,k)\right) \\ &= (UA)_{wet} \times \Delta h\end{aligned} \tag{14}$$

where,

$$\Delta h = \frac{\left(h_{a,in} - h_{fictitious}|_{T=T_{ref}(i,j,k)}\right) - \left(h_{a,exit} - h_{fictitious}|_{T=T_{ref}(i+1,j,k)}\right)}{\log \frac{h_{a,in} - h_{fictitious}|_{T=T_{ref}(i,j,k)}}{h_{a,exit} - h_{fictitious}|_{T=T_{ref}(i+1,j,k)}}} \tag{15}$$

$$\frac{1}{(UA)_{wet}} = \frac{b_w}{\eta_{overall} \times \alpha_{o,w} \times a_{node}} + \frac{b_{ref}}{\alpha_{ref} \times a_i} \tag{16}$$

$$\alpha_{o,w} = \frac{b_w \alpha_a}{Cp_a} + \frac{y_w}{k_w} \tag{17}$$

For each dry element, heat transfer rate is estimated from:

$$\begin{aligned}\Delta Q &= \dot{m}_a \times (h_{a,ex} - h_{a,in}) \\ &= \dot{m}_{ref} \times \left(h_{ref}(i,j,k) - h_{ref}(i+1,j,k)\right) \\ &= (UA)_{dry} \times \Delta T\end{aligned} \tag{18}$$

where,

$$\Delta T = \frac{\left(T_{a,in} - T_{ref}(i,j,k)\right) - \left(T_{a,exit} - T_{ref}(i+1,j,k)\right)}{\log\left[\frac{T_{a,in} - T_{ref}(i,j,k)}{T_{a,exit} - T_{ref}(i+1,j,k)}\right]} \tag{19}$$

$$\frac{1}{(UA)_{dry}} = \frac{1}{\eta_{overall} \times \alpha_a \times a_{node}} + \frac{1}{\alpha_{ref} \times a_i} \tag{20}$$

To estimate the heat transfer coefficient and pressure drop during the phase change process, it is important to understand the two-phase flow characteristics through flow-pattern maps. Cheng, Ribatski, and Thome (2008) and Cheng, Ribatski, Moreno Quibén, et al. (2008) developed a flow-pattern map of CO_2 to model correlations for frictional pressure drop and heat transfer coefficient during evaporation. These correlations are used in this study to estimate the heat transfer coefficient and pressure drop.

The general expression to estimate the heat transfer coefficient in two-phase flow:

$$\alpha_i = \alpha_{tp} = \frac{\theta_{dry}\alpha_g + (2\pi - \theta_{dry})\alpha_{wet}}{2\pi} \tag{21}$$

where θ_{dry} represents the portion in the tube covered with vapor. For annular, intermittent and bubbly flow, the tube is completely covered with liquid layer and hence $\theta_{\text{dry}} = 0$. θ_{dry} changes from zero to its maximum value for stratified-wavy flow and $\theta_{\text{dry}} = \theta_{\text{strat}}$ for stratified flow.

For the portion of the tube covered with vapor, heat transfer coefficient is estimated from:

$$\alpha_g = 0.023 \mathrm{Re}_g^{0.8} \mathrm{Pr}_g^{0.4} \frac{k_g}{d_i} \tag{22}$$

For the portion of the tube covered with a liquid layer, the heat transfer coefficient is estimated from:

$$\alpha_{wet} = \left[(S\alpha_{NB})^3 + \alpha_{CB}^3\right]^{1/3} \tag{23a}$$

where,

$$\alpha_{NB} = 131 P^{*-0.0063} (-\log P^*)^{-0.55} M^{-0.5} q''^{0.58} \tag{23b}$$

$$\alpha_{CB} = 0.0133 \mathrm{Re}_\delta^{0.69} \mathrm{Pr}_l^{0.4} \frac{k_l}{\delta_{film}} \tag{23c}$$

$$S = \begin{cases} 1, & if\ \ x < x_{IA} \\ 1 - 1.14\left(\frac{d_i}{0.00753}\right)^2 \left(1 - \frac{\delta}{\delta_{IA}}\right)^{2.2}, & if\ \ x \geq x_{IA} \end{cases} \tag{23d}$$

For mist flow, the heat transfer coefficient is estimated from:

$$\alpha_i = \alpha_M = 2 \times 10^{-8} \mathrm{Re}_H^{1.97} \mathrm{Pr}_g^{1.06} Y^{-1.83} \frac{k_g}{d_i} \tag{24a}$$

where,

$$Y = 1 - 0.1\left[\left(\frac{\rho_l}{\rho_g} - 1\right)(1 - x)\right]^{0.4} \tag{24b}$$

In the dryout region, the heat transfer coefficient is estimated from:

$$\alpha_i = \alpha_{dryout} = \alpha_{tp}(x_{di}) - \frac{x - x_{di}}{x_{de} - x_{di}} \left[\alpha_{tp}(x_{di}) - \alpha_M(x_{de})\right] \tag{25}$$

$\alpha_{tp}(x_{di})$ is the heat transfer coefficient estimated at the dryout inception quality with Equation 21 and $\alpha_M(x_{de})$ is the heat transfer coefficient estimated at the dryout completion quality with Equation 24a.

The total pressure drop of CO_2 during evaporation is estimated from:

$$\Delta P_{total} = \Delta P_{static} + \Delta P_{momentum} + \Delta P_{frictional} \tag{26}$$

where,

$$\Delta P_{static} = 0 \tag{27}$$

$$\Delta P_{momentum} = G^2 \left\{ \left[\frac{(1-x)^2}{\rho_l(1-\xi)} + \frac{x^2}{\rho_g \xi}\right]_{out} - \left[\frac{(1-x)^2}{\rho_l(1-\xi)} + \frac{x^2}{\rho_g \xi}\right]_{in} \right\} \tag{28}$$

To estimate the frictional pressure drop, different models are proposed for different flow regimes and are mentioned here.

For annular flow:

$$\Delta P_{frictional} = \Delta P_A = 4 f_A \frac{dL}{d_i} \frac{\rho_g u_g^2}{2} \tag{29a}$$

$$f_A = 3.128 \mathrm{Re}_g^{-0.454} We_l^{-0.0308} \tag{29b}$$

For slug and intermittent flow:

$$\Delta P_{frictional} = \Delta P_{slug+I} = \Delta P_{LO}\left(1 - \frac{\xi}{\xi_{IA}}\right) + \Delta P_A\left(\frac{\xi}{\xi_{IA}}\right) \tag{30a}$$

where,

$$\Delta P_{LO} = 4 f_{LO} \frac{dL}{d_i} \frac{G^2}{2\rho_l} \tag{30b}$$

$$f_{LO} = \frac{0.079}{\mathrm{Re}_{LO}^{0.25}} \tag{30c}$$

For mist flow:

$$\Delta P_{frictional} = \Delta P_M = 4 f_M \frac{dL}{d_i} \frac{G^2}{2\rho_H} \tag{31a}$$

$$f_M = \frac{91.2}{\mathrm{Re}_M^{0.832}} \tag{31b}$$

In the dryout region:

$$\begin{aligned}\Delta P_{frictional} &= \Delta P_{dryout} \\ &= \Delta P_{tp}(x_{di}) - \frac{x - x_{di}}{x_{de} - x_{di}}\left[\Delta P_{tp}(x_{di}) - \Delta P_M(x_{de})\right]\end{aligned} \tag{32}$$

where, $\Delta P_{tp}(x_{di})$ and $\Delta P_M(x_{de})$ are frictional pressure drops estimated at the dryout inception quality and dryout completion quality, respectively.

Void fraction is estimated from:

$$\xi = \frac{x}{\rho_g}\left[(1 + 0.12(1+x)) \times \left(\frac{x}{\rho_g} + \frac{(1-x)}{\rho_l}\right) + \frac{\left(1.18(1-x)[g\sigma(\rho_l - \rho_g)]^{1/4}\right)}{G\rho_l^{1/2}}\right]^{-1} \tag{33}$$

To evaluate the air-side heat transfer coefficient and pressure drop for the wet condition of the evaporator, Colburn factor "j" and friction factor "f" are estimated (Nuntaphan, Kiatsiriroat, and Wang 2005):

$$j = 0.1970 \times \mathrm{Re}_{do}^{-0.1295} \times \left(\frac{f_t}{f_p - f_t}\right)^{-0.1452} \times \left(\frac{P_l}{P_t}\right)^{1.1874} \times \left(\frac{P_t}{d_o}\right)^{0.8238} \times \left(\frac{d_f}{d_o}\right)^{0.0010} \tag{34}$$

$$f = 2.1768 \times \mathrm{Re}_{do}^{-0.2679} \times \left(\frac{f_t}{f_p - f_t}\right)^{-0.2468} \times \left(\frac{P_l}{P_t}\right)^{1.8680} \times \left(\frac{P_t}{d_o}\right)^{0.3011} \times \left(\frac{d_f}{d_o}\right)^{-0.4470} \tag{35}$$

Expansion valves

Both the electronic expansion valves are driven by feedback controllers to maintain the desired parameters. The feedback controller drives a stepper motor to adjust the longitudinal movement of a needle to maintain the desired valve opening. The expansion valves are modeled assuming an isenthalpic expansion process and the refrigerant flow rate is estimated using the flow characteristic of the expansion valves.

Calculation of total charge

To estimate the total charge in the system, the charge distribution in all the components and tubes is estimated assuming it to be a pure refrigerant.

The charge in the gas cooler is estimated from:

$$Charge_{gc} = \sum \rho_{i,j,k} a_{cross} dL_{i,j,k} \tag{36}$$

The charge in the evaporator is estimated from:

$$Charge_{ev} = Charge_{2-\phi} + Charge_{1-\phi} \tag{37}$$

$$Charge_{2-\phi} = \sum \left[\rho_g \xi + \rho_l (1-\xi)\right]_{i,j,k} a_{cross} dL_{i,j,k} \tag{38}$$

$$Charge_{1-\phi} = \sum \rho_{i,j,k} a_{cross} dL_{i,j,k} \tag{39}$$

The charge in the receiver is estimated from:

$$Charge_{rec} = \rho_g \left(\frac{V_{rec}}{H_{rec,g} + H_{rec,l}}\right) H_{rec,g} + \rho_l \left(\frac{V_{rec}}{H_{rec,g} + H_{rec,l}}\right) H_{rec,l}; \tag{40}$$

when partially filled with liquid

$$Charge_{rec} = \rho_l V_{rec}; \tag{41}$$

when completely filled with liquid

$$Charge_{rec} = \rho_g V_{rec}; \tag{42}$$

when completely filled with vapor

During simulations, constant superheat is maintained at the exit of the evaporator. Therefore, the charge in the accumulator is estimated from:

$$Charge_{acc} = \rho_{acc} V_{acc} \tag{43}$$

The connecting tubes are considered as adiabatic to estimate the amount of charge present in the tubes.

Solution procedure

The simulation model for the entire system is developed by integrating the models for individual components on MATLAB (2008) platform. The refrigerant properties are obtained from REFPROP (2010) which is integrated with the MATLAB code. To estimate the refrigerant charge, the pressure and temperature are recorded initially when the system is in standstill (switch-off mode). As the internal volume is known, from the initial pressure and temperature, the refrigerant charge is estimated. Then numerical simulations are carried out to study the effect of charge. During simulations, the calculations are initialized based on the guessed values of pressures at the discharge and suction of the compressor for both configurations. These pressures are updated by an iterative procedure. The suction pressure is updated based on the requirement of the desired superheat for both

Table 1. Ambient conditions, degree of superheat, amount of charge, and standstill system pressure for experimental tests.

				Air inlet temperature		
				Gas cooler	Evaporator	
Standstill system pressure (bar) at 32 °C	Amount of charge (g)	**Degree of superheat (K)**	Expansion stages	**DBT (°C)**	**DBT (°C)**	**WBT (°C)**
57.0	940		Double	28.61	29.74	28.88
60.2	1090		Double	28.73	29.93	28.77
61.4	1170		Double	28.65	29.74	28.84
57.0	940	12	Single	28.72	30.02	29.05
60.2	1090		Single	28.88	29.84	28.62
61.4	1170		Single	28.75	29.81	28.66
63.1	1250		Single	28.85	29.99	28.70

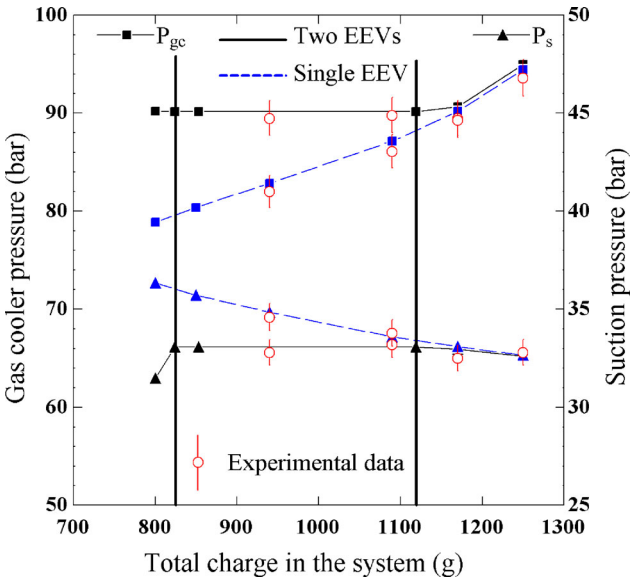

Fig. 3. Effect of refrigerant charge on gas cooler pressure and suction pressure.

cases. For the configuration with single-stage expansion, the discharge pressure is updated to get the desired amount of charge in the system. On the other hand, for the configuration with two-stage expansion, the receiver is maintained at a pressure corresponding to the saturated liquid state after the first stage of expansion. Hence, the discharge pressure is updated based on the differential pressure drop across the first expansion valve.

Results and discussion

Effect of refrigerant charge

Numerical simulations, as well as experimental tests, are performed to analyze the effect of refrigerant charge. In the experiments, the equalized pressure of the system when it is at a *standstill* condition (not in operation) is taken as an indication of the system charge. The *standstill* system pressure is recorded at identical surrounding temperatures (≈32 °C). The test conditions are shown in Table 1. It may be mentioned here that in the experimental test-rig, modeled on standard laboratory test-rigs, the state of the air at the inlet of evaporator and gas cooler is identical as the same ambient air flows thorough both these components. The experimental results reported here are for monsoon conditions, hence the air at the inlet of the evaporator is close to saturation as shown in Table 1.

Figure 3 shows the effect of refrigerant charge on gas cooler pressure and suction pressure. It is observed that for single-stage expansion, gas cooler pressure increases while suction pressure decreases with refrigerant charge. As the refrigerant charge increases, the charge accumulated in the gas cooler increases, and hence gas cooler pressure increases. With an increase in gas cooler pressure, there is an improvement in refrigerant quality at the inlet of the evaporator. This results in the requirement of a lesser refrigerant flow rate to achieve the desired superheat. Hence the flow area of the expansion valve opening decreases resulting in lesser refrigerant flow rate and lower suction pressure. On the other hand, with two-stage expansion, gas cooler pressure and suction pressure remain constant as long as the total charge is within a specific range. This is occurring because of the presence of the receiver which acts as a charge buffer. During operation, the receiver holds the charge in the form of liquid and gas. This condition must be fulfilled during operation to maintain the desired gas cooler pressure and suction pressure. There exists a range of charge over which this condition can be maintained to keep the receiver partially filled with liquid. Any variation in charge within this range will have a negligible effect on the performance of the system; as a result, the desired gas cooler pressure and the degree of superheat are effectively maintained by two EEVs. However, any change in charge beyond this range will affect the performance of the system, and no longer will the desired gas cooler pressure and the degree of superheat be maintained. For a charge higher than the upper charge limit, the liquid refrigerant completely occupies the receiver and its pressure starts increasing beyond the desired limit. While for a charge lesser than the lower charge limit, the liquid refrigerant completely disappears in the receiver and its pressure starts decreasing beyond the desired limit. With the deviation of receiver pressure from the desired

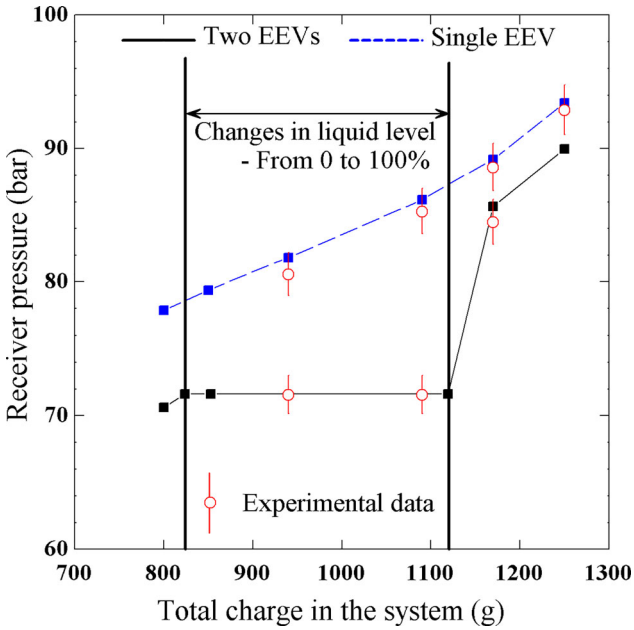

Fig. 4. Effect of refrigerant charge on receiver pressure.

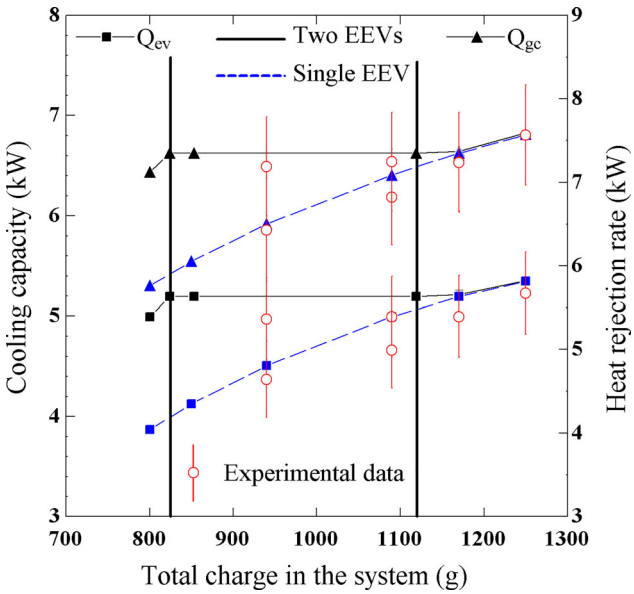

Fig. 5. Effect of refrigerant charge on cooling capacity and heat rejection rate.

limit, the performance of the system gets affected and the desired gas cooler and suction pressures are no longer maintained. This phenomenon is presented in Figures 3 and 4.

The receiver pressure is the same as the gas cooler pressure with single-stage expansion (Figure 4). Conversely, for the configuration with two-stage expansion, the receiver is maintained at a pressure corresponding to the saturated liquid state (Figure 4). At that pressure, it is also essential to keep the receiver partially filled with liquid. Results show that the liquid level inside the receiver changes from 0 to 100%, as the charge is changed within the system. Hence, it is possible to maintain the desired receiver pressure over a range of charge.

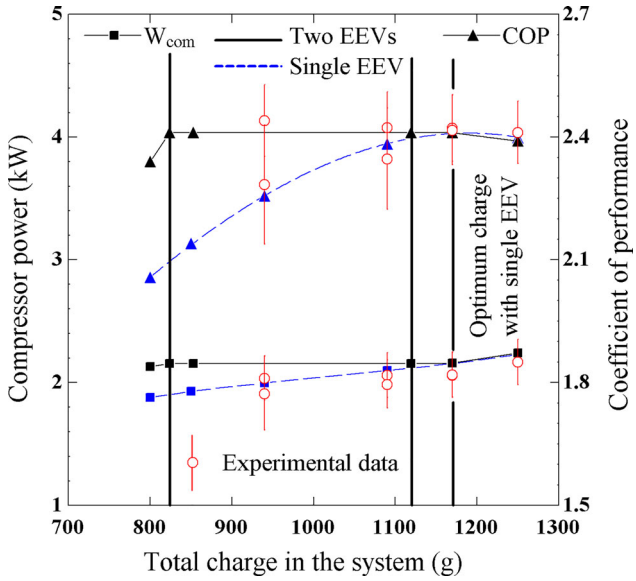

Fig. 6. Effect of refrigerant charge on compressor power and COP.

Figure 5 shows the effect of refrigerant charge on cooling capacity and heat rejection rate. For single-stage expansion, it is observed that with an increase in refrigerant charge, there is an improvement in the refrigerant quality at the inlet of the evaporator. As a result, the specific enthalpy difference across the evaporator increases leading to an increase in cooling capacity. Similarly, the heat rejection rate increases due to an increase in specific enthalpy difference across the gas cooler. On the other hand, in the case of the configuration with two-stage expansion, the performance of the system is insensitive to any changes in charge within a specific range. Hence, cooling capacity and heat rejection rate remain the same as long as the charge is within the specific range.

Figure 6 shows the effect of refrigerant charge on compressor power and COP. It is observed that with single-stage expansion, maximum COP is obtained for the optimum charge maintained in the system. However, with two-stage expansion, maximum COP is obtained over a range of refrigerant charge.

Receiver size and its effect on the performance of the system with two-stage expansion

Results above show that for two-stage expansion, there exists a range of refrigerant charge over which the liquid portion in the receiver changes from 0 to 100%. For any change in charge beyond this range, no longer will the desired receiver pressure be maintained and the performance of the system deviates from optimum. Hence it is essential to properly select the size of the receiver as well as the refrigerant charge. In the present study, numerical simulations are carried out considering different sizes of the receiver and by varying the refrigerant charge. Results show that for each size of the receiver, there is a range of refrigerant charge over which the liquid portion changes from 0 to 100% in the receiver. Higher the size of the receiver, higher will be the range of refrigerant charge over which the liquid portion changes from 0 to 100% in the receiver. For different

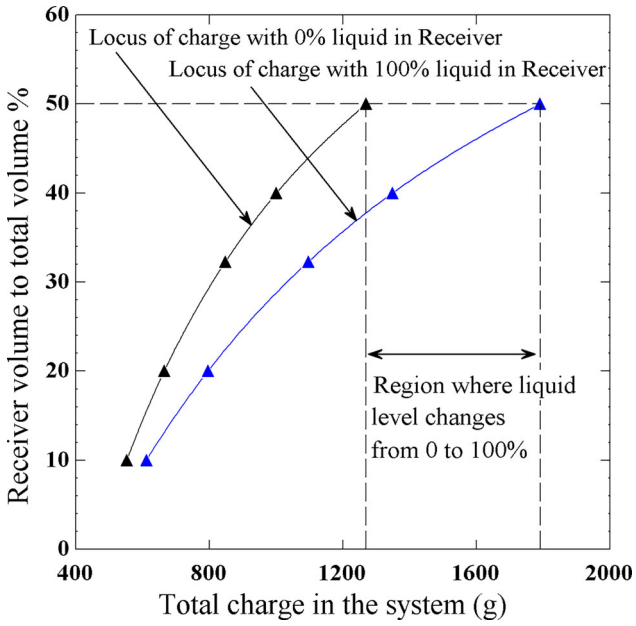

Fig. 7. Loci of charge with 0% and 100% liquid in receiver for different sizes of receiver.

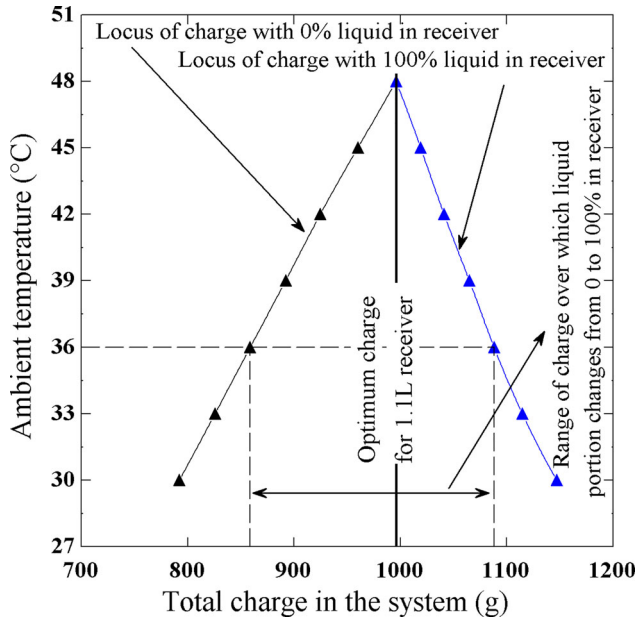

Fig. 8. Loci of charge with 0% and 100% liquid in receiver at different ambient temperatures.

sizes of the receiver, the loci are drawn with 0% liquid and 100% liquid in the receiver (Figure 7). It is observed that for a receiver size of 50% of total system volume including the volume of the receiver, the liquid portion in the receiver changes from 0 to 100% for changes in charge from 1270 g to 1790 g. Thus for a specific size of the receiver, the refrigerant charge should be maintained within the range to keep the receiver partially filled with liquid during operation. This may call for a tradeoff between the receiver size and acceptable charge variation. Smaller receivers are acceptable if the expected charge variation is small. For example, for residential air conditioners, the leakages are expected to be small, hence smaller receiver is adequate. Whereas for mobile air conditioning, larger receivers may be needed as the leakages are expected to be higher.

Effect of ambient temperature

The effect of ambient temperature on the performance of the system is analyzed in this section. To perform this study, numerical simulations are carried out at different ambient temperatures.

As discussed in the preceding section, at a specific ambient temperature, there is a range of charge over which the liquid portion changes from 0 to 100% in the receiver for the configuration with two-stage expansion. This gives the benefit of maintaining the optimum performance with two-stage expansion over a range of charge at a specific ambient temperature. It is observed that this range contracts as the ambient temperature increases (Figure 8). With an increase in ambient temperature, the refrigerant temperature at the exit of gas cooler increases, and therefore the state obtained at the exit of the first stage of expansion approaches critical point (Figure 9). As a result, the density of liquid refrigerant and the density of vapor refrigerant approach each other

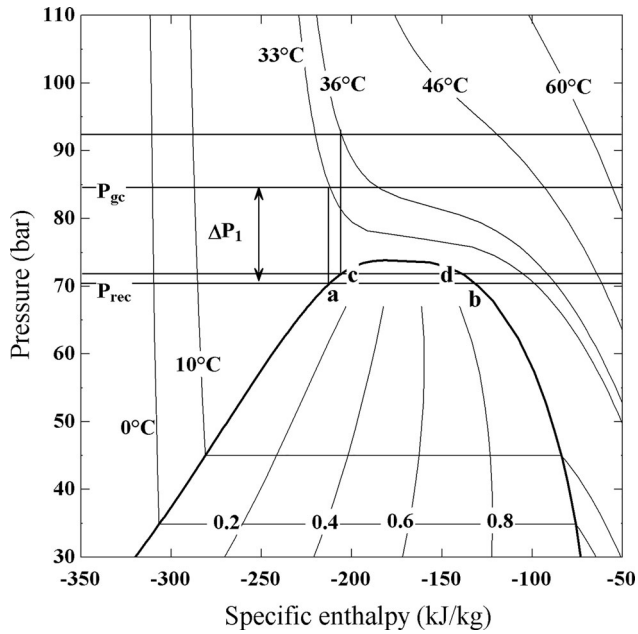

Fig. 9. Representation of expansion in 1st EEV for the configuration with two-stage expansion.

(Figure 9) thereby reducing the range of charge over which the liquid portion changes from 0 to 100% in the receiver. This range disappears at the critical point. Figure 8 shows the loci of refrigerant charge with 0% liquid and 100% liquid in the receiver for varying ambient temperatures. It is observed that for an ambient temperature of 48 °C, the exit state of the first stage of expansion falls on the critical point and therefore the locus of 0% liquid in receiver merges with the locus of 100% liquid in the receiver. The refrigerant charge for which the exit state of the first stage of expansion

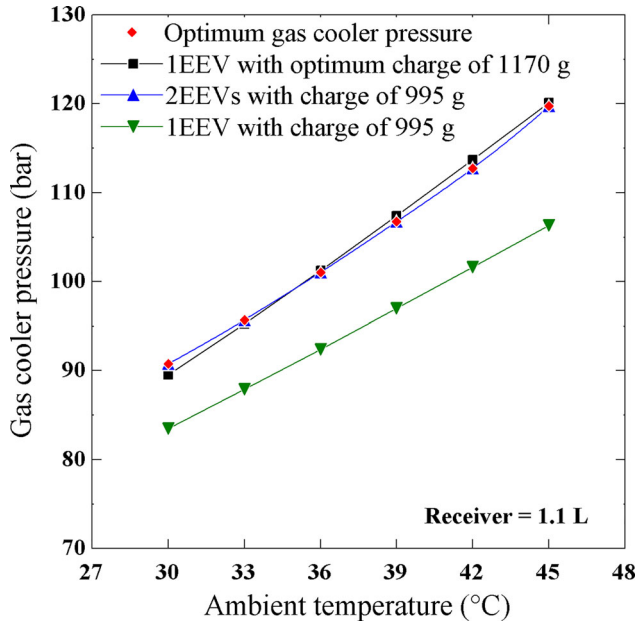

Fig. 10. Effect of ambient temperature on gas cooler pressure.

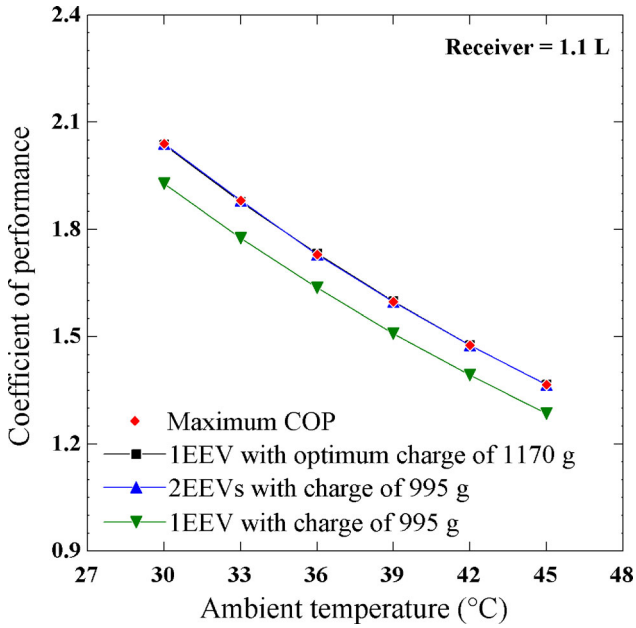

Fig. 11. Effect of ambient temperature on COP.

falls on the critical point should be treated as optimum charge for the given system with two-stage expansion. With this optimum charge maintained in the given system with two-stage expansion, it is possible to track the optimum system's performance with changes in ambient temperatures effectively.

This study also presents the effect of ambient temperature on gas cooler pressure and COP of the system. The optimum gas cooler pressure that gives the maximum COP for the given system is first predicted from numerical simulations. Results are plotted in Figures 10 and 11. Next, numerical simulations are carried out for the configurations with single-stage expansion as well as two-stage expansion to investigate the effect of ambient temperature on gas cooler pressure and COP for the respective configurations. These results are compared with the optimum gas cooler pressure and maximum COP. It is observed that the configuration with single-stage expansion tracks the optimum gas cooler pressure effectively at different ambient temperatures with an optimum charge of 1170 g maintained in the system (Figure 10). Similarly, for the configuration with two-stage expansion, it is possible to maintain the optimum gas cooler pressure at different ambient temperatures with an optimum charge of 995 g maintained in the given system (Figure 10). The COPs obtained for the systems with single-stage expansion as well as two-stage expansion, overlap with the maximum COP (Figure 11) when optimum charges are maintained in the respective systems. For the system with single-stage expansion, the gas cooler pressure as well as COP deviates from the optimum values (Figure 11) when the refrigerant charge in the system is reduced to 995 g. From this discussion, it can be seen that for the same performance, the required charge can be reduced by about 15% when using 2-stage expansion as compared to 1-stage expansion. The explanation for this observation is discussed here. With the single-stage expansion, there exists an optimum charge that needs to be maintained to achieve the optimum performance of the system at different ambient temperatures. This optimum charge is 1170 g for the present system. Conversely, for the configuration with two-stage expansion, there exists a range of charge over which the optimum performance is maintained at a specific ambient temperature. However, this range contracts with an increase in ambient temperature (Figure 8), and finally for an ambient temperature of 48 °C, the range disappears. The refrigerant charge corresponding to this state is 995 g. This refrigerant charge for which the range disappears should be treated as the optimum charge for the configuration with two-stage expansion. Thus it is observed that the optimum charge for two-stage expansion system is 15% lower than the optimum charge for single-stage expansion system.

Conclusions

To investigate the sensitivity in the performance of a transcritical CO_2 based system with varying refrigerant charge, experimental and numerical studies are carried out. Two configurations are considered for the present system—one with single-stage expansion and the other with two-stage expansion.

From the theoretical and experimental studies, the following conclusions are drawn:

1. The configuration with the single-stage expansion is more sensitive to refrigerant charge compared to the configuration with two-stage expansion. For single-stage expansion, there is an optimum charge at which the COP is maximum.
2. For two-stage expansion, maximum COP is maintained over a larger range of refrigerant charge for a given

internal volume and operating conditions. This indicates that this configuration is more suitable in applications where refrigerant leakages are higher.

3. Proper sizing of the receiver is essential for the configuration with two-stage expansion to maintain the optimum performance over a wide range of operating conditions. It is observed that the higher the size of the receiver, the higher will be the range of refrigerant charge over which the optimum performance is maintained for two-stage expansion.
4. This study also presents the effect of ambient temperature on the performance of both configurations with single-stage as well as two-stage expansion. Results show that both configurations can effectively track the optimum performance at different ambient temperatures with optimum charge maintained in the respective configurations.
5. It is observed that for the same performance, the required charge can be reduced by about 15% for the configuration with two-stage expansion as compared to single-stage expansion.
6. Besides, it is observed that the configuration with two-stage expansion offers better system controllability, provided the receiver is sized properly.

Nomenclature

a = [m^2] Surface area of a heat exchanger element
C = [W K^{-1}] Capacity rate
C_p = [J kg^{-1} K^{-1}] Specific heat at constant pressure
d = [m] Diameter
dL = [m] Length of an element
f = [-] Friction factor
G = [kg m^{-2} s^{-1}] Mass flux
H = [m] Height
h = [J kg^{-1}] Specific enthalpy
j = [-] Colburn factor
k = [W m^{-1} K^{-1}] Thermal conductivity
M = [kg $kmol^{-1}$] Molecular weight
$\dot{m}$ = [kg s^{-1}] Mass flow rate
Nu = [-] Nusselt number
P = [Pa] Pressure
P^* = [-] Reduced pressure
Pr = [-] Prandtl number
Q = [W] Heat transfer rate
q'' = [W m^{-2}] Heat flux
Re = [-] Reynolds number
T = [K] Temperature
u = [m s^{-1}] Velocity
V = [m^3] Volume
W = [W] Compressor power
We = [-] Weber number
x = [-] Vapor quality

Special characters

ρ = [kg m^{-3}] Density
α = [W m^{-2} K^{-1}] Heat transfer coefficient
ε = [-] Effectiveness
ξ = [-] Void fraction
σ = [N m^{-1}] Surface tension
θ = [rad] Angle of tube perimeter
η = [-] Efficiency
ϕ = [-] Phase

Subscripts

acc = Accumulator
a = Air
d = Discharge
ex = Exit
ev = Evaporator
f = Fin
gc = Gas cooler
g = Gas
i = Inner
in = Inlet
l = Liquid
min = Minimum
max = Maximum
o = Outer
ref = Refrigerant
rec = Receiver
s = Suction
w = Water

Funding

Science and Engineering Research Board, DST, India.

References

Aprea, C., A. Greco, and A. Maiorino. 2015. An experimental study on charge optimization of a trans-critical CO_2 cycle. *International Journal of Environmental Science and Technology* 12 (3): 1097–106. doi:10.1007/s13762-014-0502-6

Baek, C., J. Heo, J. Jung, H. Cho, and Y. Kim. 2013. Optimal control of the gas-cooler pressure of a CO_2 heat pump using EEV opening and outdoor fan speed in the cooling mode. *International Journal of Refrigeration* 36 (4):1276–84. doi:10.1016/j.ijrefrig.2013.02.009

Boccardi, G., N. Calabrese, G. P. Celata, R. Mastrullo, A. W. Mauro, A. Perrone, and R. Trinchieri. 2013. Experimental performance evaluation for a carbon dioxide light commercial cooling application under transcritical and subcritical conditions. *Applied Thermal Engineering* 54 (2):528–35. doi:10.1016/j.applthermaleng.2013.02.026

Bush, J., M. Beshr, V. Aute, and R. Radermacher. 2017. Experimental evaluation of transcritical CO_2 refrigeration with mechanical subcooling. *Science and Technology for the Built Environment* 23 (6):1013–25. doi:10.1080/23744731.2017.1289056

Cabello, R., D. Sanchez, R. Llopis, and E. Torrella. 2008. Experimental evaluation of the energy efficiency of a CO_2 refrigerating plant working in transcritical conditions. *Applied Thermal Engineering* 28 (13):1596–604. doi:10.1016/j.applthermaleng.2007.10.026

Cao, F., Z. Ye, and Y. Wang. 2020. Experimental investigation on the influence of internal heat exchanger in a transcritical CO_2 heat

pump water heater. *Applied Thermal Engineering* 168:114855. doi:10.1016/j.applthermaleng.2019.114855

Casson, V., L. Cecchinato, M. Corradi, E. Fornasieri, S. Girotto, S. Minetto, L. Zamboni, and C. Zilio. 2003. Optimisation of the throttling systm in a CO_2 refrigerating machine. *International Journal of Refrigeration* 26 (8):926–35. doi:10.1016/S0140-7007(03)00077-X

Catalán-Gil, J., R. Llopis, D. Sánchez, L. Nebot-Andrés, and R. Cabello. 2019. Energy analysis of dedicated and integrated mechanical subcooled CO_2 boosters for supermarket applications. *International Journal of Refrigeration* 101:11–23. doi:10.1016/j.ijrefrig.2019.01.034

Cheng, L., G. Ribatski, J. Moreno Quibén, and J. R. Thome. 2008. New prediction methods for CO_2 evaporation inside tubes: Part I—A two-phase flow pattern map and a flow pattern based phenomenological model for two-phase flow frictional pressure drops. *International Journal of Heat and Mass Transfer* 51 (1-2): 111–24. doi:10.1016/j.ijheatmasstransfer.2007.04.002

Cheng, L., G. Ribatski, and J. R. Thome. 2008. New prediction methods for CO_2 evaporation inside tubes: Part II—An updated general flow boiling heat transfer model based on flow patterns. *International Journal of Heat and Mass Transfer* 51 (1-2):125–35. doi:10.1016/j.ijheatmasstransfer.2007.04.001

Cho, H., C. Ryu, and Y. Kim. 2007. Cooling performance of a variable speed CO_2 cycle with an electronic expansion valve and internal heat exchanger. *International Journal of Refrigeration* 30 (4): 664–71. doi:10.1016/j.ijrefrig.2006.10.004

Cho, H., C. Ryu, Y. Kim, and H. Y. Kim. 2005. Effects of refrigerant charge amount on the performance of a transcritical CO_2 heat pump. *International Journal of Refrigeration* 28 (8):1266–73. doi:10.1016/j.ijrefrig.2005.09.011

Elbel, S., and N. Lawrence. 2016. Review of recent developments in advanced ejector technology. *International Journal of Refrigeration* 62:1–18. doi:10.1016/j.ijrefrig.2015.10.031

Groll, E. A., and J. H. Kim. 2007. Review article: Review of recent advances toward transcritical CO_2 cycle technology. *HVAC&R Research* 13 (3):499–520. doi:10.1080/10789669.2007.10390968

Gullo, P., A. Hafner, and K. Banasiak. 2018. Transcritical R744 refrigeration systems for supermarket applications: Current status and future perspectives. *International Journal of Refrigeration* 93 (2018):269–310. doi:10.1016/j.ijrefrig.2018.07.001

Hazarika, M. M., M. Ramgopal, and S. Bhattacharyya. 2018. Studies on a transcritical R744 based summer air-conditioning unit: Impact of refrigerant charge on system performance. *International Journal of Refrigeration* 89:22–39. doi:10.1016/j.ijrefrig.2018.03.007

He, Y. J., X. Y. Liang, J. H. Cheng, L. L. Shao, and C. L. Zhang. 2020. Approaching optimum COP by refrigerant charge management in transcritical CO_2 heat pump water heater. *International Journal of Refrigeration* 118:161–72. doi:10.1016/j.ijrefrig.2020.06.011

Hou, Y., J. Ma, C. Liu, J. Cao, and X. Liu. 2014. Experimental investigation on the influence of EEV opening on the performance of transcritical CO_2 refrigeration system. *Applied Thermal Engineering* 65 (1-2):51–6. doi:10.1016/j.applthermaleng.2013.12.054

Karampour, M., and S. Sawalha. 2018. State-of-the-art integrated CO_2 refrigeration system for supermarkets: A comparative analysis. *International Journal of Refrigeration* 86:239–57. doi:10.1016/j.ijrefrig.2017.11.006

Lawrence, N., and S. Elbel. 2015. Analysis of two-phase ejector performance metrics and comparison of R134a and CO_2 ejector performance. *Science and Technology for the Built Environment* 21 (5):515–25. doi:10.1080/23744731.2015.1030327

Lin, K. H., C. S. Kuo, W. D. Hsieh, and C. C. Wang. 2013. Modeling and simulation of the transcritical CO_2 heat pump system. *International Journal of Refrigeration* 36 (8):2048–64. doi:10.1016/j.ijrefrig.2013.08.008

Llopis, R., L. Nebot-Andrés, R. Cabello, D. Sánchez, and J. Catalán-Gil. 2016. Experimental evaluation of a CO_2 transcritical refrigeration plant with dedicated mechanical subcooling. *International Journal of Refrigeration* 69:361–8. doi:10.1016/j.ijrefrig.2016.06.009

Lorentzen, G., and J. Pettersen. 1993. A new, efficient and environmentally benign system for car air-conditioning. *International Journal of Refrigeration* 16 (1):4–12. doi:10.1016/0140-7007(93)90014-Y

MATLAB. 2008. *The MathWorks, Inc*. (version 7.6.0). Natick, MA.

Nebot-Andrés, L., J. Catalán-Gil, D. Sánchez, D. Calleja-Anta, R. Cabello, and R. Llopis. 2020. Experimental determination of the optimum working conditions of a transcritical CO_2 refrigeration plant with integrated mechanical subcooling. *International Journal of Refrigeration* 113:266–75. doi:10.1016/j.ijrefrig.2020.02.012

Nuntaphan, A., T. Kiatsiriroat, and C. C. Wang. 2005. Heat transfer and friction characteristics of crimped spiral finned heat exchangers with dehumidification. *Applied Thermal Engineering* 25 (2-3):327–40. doi:10.1016/j.applthermaleng.2004.05.014

Pitla, S. S., E. A. Groll, and S. Ramadhyani. 2002. New correlation to predict the heat transfer coefficient during in-tube cooling of turbulent supercritical CO_2. *International Journal of Refrigeration* 25 (7):887–95. doi:10.1016/S0140-7007(01)00098-6

Pongsoi, P., P. Promoppatum, S. Pikulkajorn, and S. Wongwises. 2013. Effect of fin pitches on the air-side performance of L-footed spiral fin-and-tube heat exchangers. *International Journal of Heat and Mass Transfer* 59 (1):75–82. doi:10.1016/j.ijheatmasstransfer.2012.11.071

REFPROP. 2010. *Thermodynamic properties of refrigerants and refrigerant mixures, version 9.0*. Gaithersberg, MD: National Institute of Standards and Technology.

Threlkeld, J. L. 1970. *Thermal environmental engineering*. New York, NY: Prentice-Hall Inc.

Wang, D., Z. Zhang, B. Yu, X. Wang, J. Shi, and J. Chen. 2019. Experimental research on charge determination and accumulator behavior in trans-critical CO_2 mobile air-conditioning system. *Energy* 183:106–15. doi:10.1016/j.energy.2019.06.116

Wang, S., H. Tuo, F. Cao, and Z. Xing. 2013. Experimental investigation on air-source transcritical CO_2 heat pump water heater system at a fixed water inlet temperature. *International Journal of Refrigeration* 36 (3):701–16. doi:10.1016/j.ijrefrig.2012.10.011

Yin, J. M., C. W. Bullard, and P. S. Hrnjak. 2001. R-744 gas cooler model development and validation. *International Journal of Refrigeration* 24 (7):692–701. doi:10.1016/S0140-7007(00)00082-7

Zhu, J., and S. Elbel. 2020. Experimental investigation into the influence of vortex control on transcritical R744 ejector and cycle performance. *Applied Thermal Engineering* 164:114418. doi:10.1016/j.applthermaleng.2019.114418